Available online at www.sciencedirect.com
ScienceDirect
Journal of Power Sources 161 (2006) 203–213
JOURNAL OF POWER SOURCES
www.elsevier.com/locate/jpowsour

# Simulation of the water and heat management in proton exchange membrane fuel cells

Luis Matamoros*, Dieter Brüggemann

*Lehrstuhl für Technische Thermodynamik und Transportprozesse, Universität Bayreuth, 95440 Bayreuth, Germany*

Received 20 January 2006; received in revised form 28 February 2006; accepted 22 March 2006
Available online 18 May 2006

**Abstract**

A non-isothermal and three-dimensional numerical model of a PEM fuel cell was developed to compute the water and heat management. Transport of water in the polymer membrane, phase change of water in the cathode porous medium and capillary flow to the gas channels were determined. Influences of these phenomena on fuel cells and conditions that may affect their performance have been numerically evaluated. Output variables are velocity, temperature, mass fraction, current density, voltage loss, water content of the polymer membrane, saturation and liquid flow fields. Cell voltage and total current density of PEM fuel cell were computed as well. Results show that there may be severe mass transfer limitations depending either on the design or on the water management of the cell. For the chosen conditions, the polymer membrane can keep and even increase its water content, as long as inlet flows are injected at 100% relative humidity. In case the fuel cell is operated under dehydrating conditions, the decrease of the water content of the polymer electrolyte may affect the performance. The variations of temperature were small. However, temperature plays an important role in the cathode reaction rate of the cell and in the dehydration of the polymer membrane. Numerical results and experimental data were found to be in good agreement.


*Keywords:* PEM fuel cells; Model; Polymer membrane; Saturation

## 1. Introduction

The performance of PEM fuel cells depends highly on the water content of the polymer membrane, which is inversely proportional to the proton resistance. Therefore, decreasing water content leads to a diminishing of performance due to the increase of the voltage loss in the membrane. In addition to this point, dehydrating conditions in PEM fuel cells may not only affect the proton resistance of the membrane, but also the proton resistance of the polymer electrolyte contained in the cathode catalyst layer. Then, the cathode reaction rate is affected by changes of local cathode overpotential caused by high proton resistance [1,2].

Therefore, to avoid dehydration of the polymer electrolyte, the inlet flows are usually injected as a mixture with water vapor at a certain temperature. However, produced water and lack of diffusion flux for the disposal of this water may cause condensation in the cathode porous medium, which may clog pores and block the transport of species to reactive sites. For these reasons, the management of water in the PEM fuel cell becomes highly important.

In order to achieve a complete solution of the transport phenomena in PEM fuel cells, the water management, which in turn requires the consideration of the heat management, must be accurately taken into account. In order to establish the influence of the water on the performance of the fuel cell, the water movement in the polymer membrane as well as the condensation and capillary flow in the cathode gas diffusion layer and catalyst layer should be properly estimated. Finally, the flow field in the gas channel should be able to dispose the condensed water. If these aspects are neglected, numerical results may be erroneous, given that the behavior of the whole system is highly dependant on the liquid and gaseous water transport.

Many approaches for calculation of one, two and three dimensional variations of important properties inside PEM fuel cells have been made. However, each approach put emphasis on different aspects. Wang's review [3] shows a complete description of the most important models created for the calculation of different variables involved in PEM fuel cells. Up to now, some

* Corresponding author. Tel.: +49 921 557168; fax: +49 921 557165.
*E-mail address:* luis.matamoros@uni-bayreuth.de (L. Matamoros).

0378-7753/$ – see front matter © 2006 Elsevier B.V. All rights reserved.
doi:10.1016/j.jpowsour.2006.03.078

## Nomenclature

| | |
|---|---|
| $A_{LG}/V_L$ | gas–liquid interfacial area ($m^{-1}$) |
| $A_{superf}$ | Pt area per Pt mass ($m^2\,kg^{-1}$) |
| ARH | anode relative humidity |
| $c_p$ | volumetric thermal capacity ($J\,kg^{-1}\,K^{-1}$) |
| $C$ | molar concentration ($kmol\,m^{-3}$) |
| $C_{O_2ref}$ | oxygen reference molar concentration ($kmol\,m^{-3}$) |
| $C_{O_2s}$ | oxygen molar concentration at the agglomerate surface ($kmol\,m^{-3}$) |
| CRH | cathode relative humidity |
| $D$ | diffusivity ($m^2\,s^{-1}$) |
| $F$ | Faraday constant |
| $g$ | gravity acceleration ($m\,s^{-2}$) |
| $i_{oref}$ | reference exchange current density ($A\,m^{-2}$) |
| $k$ | thermal conductivity ($W\,m^{-1}\,K^{-1}$) |
| $K_p$ | hydraulic permeability ($m^2$) |
| $m_{pt}$ | Pt mass per volume ($kg\,m^{-3}$) |
| $M$ | molecular weight ($kg\,kmol^{-1}$) |
| $\dot{n}_{GLH_2O}$ | volumetric condensation rate ($kg\,s^{-1}m^{-3}$) |
| $N$ | molar flux ($mol\,m^{-2}\,s^{-1}$) |
| $N_{Drag}$ | electro-osmotic drag factor ($mol_{H_2O}(mol_{H^+})^{-1}$) |
| $P$ | pressure (Pa) |
| $r$ | reaction rate ($kmol\,s^{-1}\,m^{-3}$) |
| $R$ | universal constant of gases |
| $R_{agg}$ | agglomerate ratio (m) |
| $s$ | liquid saturation |
| $S_i$ | source term of species $i$ |
| $S_m$ | source term of mass |
| $S_T$ | source term of energy |
| $S_V$ | source term of momentum |
| $T$ | temperature (K) |
| $V$ | velocity ($m\,s^{-1}$) |
| $x$ | molar fraction |
| $y$ | mass fraction |

*Greek*

| | |
|---|---|
| $\alpha_c$ | transfer coefficient cathode side |
| $\epsilon$ | porosity |
| $\eta$ | cathode overpotential (V) |
| $\theta$ | contact angle (rad) |
| $\lambda$ | water content ($mol_{H_2O}(mol_{SO_3^-})^{-1}$) |
| $\mu$ | dynamic viscosity ($kg\,m^{-1}\,s^{-1}$) |
| $\varrho$ | density ($kg\,m^{-3}$) |
| $\sigma$ | surface tension ($N\,m^{-1}$) |

*Subscripts*

| | |
|---|---|
| agg | agglomerate |
| c | capillary |
| G | gas |
| $H^+$ | proton |
| $H_2O$ | water |
| $i$ | species $i$ |
| $j$ | species $j$ |
| L | liquid |
| m | mixture |
| $O_2$ | oxygen |
| S | solid |
| $SO_3^-$ | sulfonate group |

models have been provided to estimate the movement of liquid and gaseous water in the cathode porous medium of the fuel cell [2,4–7].

The objective of this work is to present a numerical solution of the water and heat management in PEM fuel cells. The polymer membrane is considered as a component highly affected by its external conditions, hence the mass transfer between the membrane, the cathode and the anode porous mediums is taken into account, in order to determine the actual water content field, so the actual voltage losses and the cathode electrolyte overpotential are obtained. The liquid water saturation factor in the porous medium is estimated by relations based on the kinetic theory of gases and by the Leverett function for the capillary movement of liquid in unsaturated hydrophobic porous mediums [2,4,6,7].

## 2. Model description

A simple straight PEM fuel cell was taken as computational domain, given that the main purpose of this work is to study the transport behavior of the species in each component. Using a symmetry assumption, the domain was vertically split in two parts and only the left part was calculated (Fig. 1). The model is three-dimensional and simultaneously calculates the behavior of gas channels, catalyst layers and polymer membrane.

### 2.1. Fundamental equations

In order to obtain the velocity fields, the Navier–Stokes equations were used in the following form:

$$V \cdot \nabla \varrho V = -\nabla P + \nabla \mu \nabla V + S_V \quad (1)$$

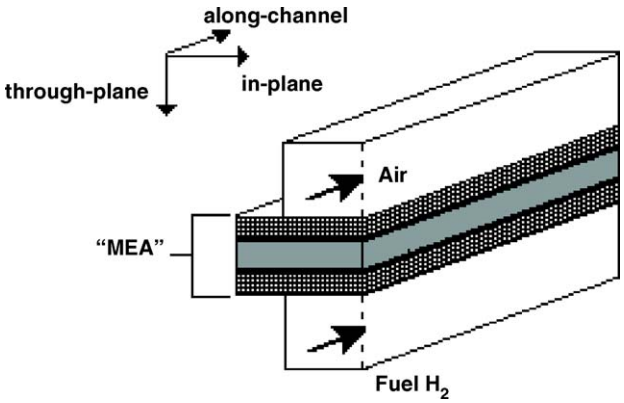


Fig. 1. Control volume for the numerical solution.

The energy balance is expressed as

$$V \cdot \nabla \varrho c_p T = -\nabla k \nabla T + S_T \tag{2}$$

and the species mass balance is represented by

$$V \cdot \nabla \varrho y_i = -\nabla D_{i,\mathrm{m}} \nabla \varrho y_i + S_i \tag{3}$$

Finally, each equation is coupled with the continuity equation:

$$\nabla \varrho V = S_\mathrm{m} \tag{4}$$

For the polymer membrane, a water content balance was made in order to consider electro-osmotic drag and back diffusion of water molecules:

$$\nabla D_\lambda \nabla \lambda = \frac{M_{\mathrm{SO}_3^-}}{\varrho_{\mathrm{SO}_3^-}} \frac{\mathrm{d}N_\mathrm{Drag} N_{\mathrm{H}^+}}{\mathrm{d}x} \tag{5}$$

Two-phase flow in the cathode porous medium (gas diffusion layer and catalyst layer) is assumed as separated phases. Berning and Djilali [6] proposed a liquid water velocity field considering both convection and capillary forces. In this work, the liquid is assumed to flow individually driven by capillary pressure gradients, produced by gradients of liquid saturation and surface tension [5,7], and so, convection is neglected in porous mediums. The capillary pressure is semi-empirically calculated by means of the Leverett function $J(S)$ for hydrophobic unsaturated porous mediums [2,7]:

$$P_\mathrm{c} = \frac{\sigma \cos\theta}{(K_p/\epsilon)^{1/2}} J(S) \tag{6}$$

The Leverett function $J(S)$ for hydrophobic porous mediums is expressed as

$$J(S) = 1.417S - 2.120S^2 + 1.263S^3 \tag{7}$$

where the reduced saturation factor $S$ is the following:

$$S = \frac{s - s_\mathrm{im}}{1 - s_\mathrm{im}} \tag{8}$$

Below the saturation value $s_\mathrm{im}$ (immobile saturation), the water is assumed to be a discontinuous flow pattern, and so, the capillary flow is neglected. At the gas channel, liquid water is disposed either by high convective air flow or by evaporation. Then, the reduced saturation factor is assumed to be zero at the gas channel and gas diffusion layer interface [7].

To determine the phenomenological behavior of the liquid in the porous medium, Darcy's law is used:

$$\nabla \frac{\varrho_{\mathrm{H_2O(L)}} K_p S^3}{\mu_{\mathrm{H_2O(L)}}} \left(\frac{\mathrm{d}P_\mathrm{c}}{\mathrm{d}S}\right) \nabla S = \dot{n}_{\mathrm{GLH_2O}} \tag{9}$$

In order to calculate the change of phase of water to establish the saturation factor in porous medium, the condensation kinetic theory is used to determine the volumetric condensation rate $\dot{n}_{\mathrm{GLH_2O}}$ expressed as

$$\dot{n}_{\mathrm{GLH_2O}} = K_\mathrm{GL} M_{\mathrm{H_2O}} \frac{A_\mathrm{LG}}{V_\mathrm{L}} \frac{P_{\mathrm{H_2O(G)}} - P^\mathrm{Sat}_{\mathrm{H_2O}}}{RT} \tag{10}$$

The factor $K_\mathrm{GL}$ consists of the diffusion terms for the condensation process [7]. The evaporation was assumed to be the inverse of the condensation process. The gas–liquid interfacial area $A_\mathrm{LG}/V_\mathrm{L}$ was arbitrarily assumed as constant.

All equations of balance are discretisized and solved simultaneously using the Jacobi–Gauss–Seidel relaxation iterative numerical method. This method and boundary conditions were written in Fortran90 for calculation of the output parameters of the model.

### 2.2. Transport properties

The density of gases is calculated using the ideal gas equation. Dynamic viscosity and thermal conductivity are determined using the kinetic theory of gases.

The thermal conductivities are expressed as an average between conductivities of phases involved in each infinitesimal element of the system:

$$k = k_\mathrm{S} f(1-\epsilon) + k_\mathrm{G} f(\epsilon)(1-s) + k_\mathrm{L} f(\epsilon) s \tag{11}$$

The volumetric thermal capacity is also regarded as an average between phases. Consequently, thermal equilibrium between phases is assumed:

$$c_p = c_{p\mathrm{S}}(1-\epsilon) + c_{p\mathrm{G}}\epsilon(1-s) + c_{p\mathrm{L}}\epsilon s \tag{12}$$

In order to consider the influence of the porous medium on the conductive heat transport, the following correction factors (Eqs. 13 and 14) were used for the catalyst layers and the gas diffusion layers, respectively [8]:

$$f(\epsilon) = \epsilon^{1.5} \tag{13}$$

$$f(\epsilon) = \epsilon \left(\frac{\epsilon - \epsilon_\beta}{1 - \epsilon_\beta}\right)^\alpha \tag{14}$$

The factor $\epsilon_\beta$ is considered as 0.11 and $\alpha$ is 0.527 for in-plane diffusion and 0.785 for cross-plane diffusion [7].

The mixture diffusivity was approximated by the mixture rule [9]:

$$D_{i,\mathrm{m}} = \frac{\sum_{i=1, i\neq j}^{n} x_i M_i}{\sum_{i=1}^{n} x_i M_i \sum_{i=1, i\neq j}^{n} (x_i / D_{i,j})} \tag{15}$$

The binary diffusivities were calculated using the following correlation for gases at low density [9]:

$$\frac{PD_{i,j}}{(P_{\mathrm{c}i} P_{\mathrm{c}j})^{1/3} (T_{\mathrm{c}i} T_{\mathrm{c}j})^{5/12} ((1/M_i) + (1/M_j))^{1/2}} = a \left(\frac{T}{\sqrt{T_{\mathrm{c}i} T_{\mathrm{c}j}}}\right)^b \tag{16}$$

in this equation, $a$ and $b$ are constant. If the mixture diffusivity is calculated for a porous medium, Eqs. (13) and (14) are used to account for the effect of porosity and tortuosity of the catalyst layer and the gas diffusion layer, respectively. The effect of the liquid water saturation is accounted for by using a normalized function $f(s) = (1-s)^{1.5}$. Therefore, the final form of the diffusivity is

$$D_{i,\text{m-corrected}} = D_{i,\mathrm{m}} f(\epsilon) f(s) \tag{17}$$

For the polymer electrolyte, the electro-osmotic drag coefficient $N_{\mathrm{Drag}}$ was calculated at 30 and 80 °C using the empirical data for Nafion from Springer et al. [10] and Neubrand [11], respectively. Diffusion coefficient of water $D_\lambda$ was calculated at 30 and 80 °C from the empirical data for Nafion of Zawodzinski et al. [12] and Neubrand [11], respectively.

### 2.3. Boundary conditions

The thermal boundary conditions between flow and channel's walls may be considered as either adiabatic or isothermal.

The water content of the polymer electrolyte was assumed to be highly affected by external conditions. Therefore, a simple theory was considered suitable for determining the interfacial mass transfer between the cathode and anode porous mediums and polymer membrane. The water transport between the catalyst layer and the polymer membrane is driven by the difference between the bulk concentrations in each phase and the equilibrium concentrations of water in the interface. In this work the interfacial mass transfer relation of the molar fraction of each phase ($Y_i$ and $X_i$) and the mixture diffusivity of the species $i$ by each phase ($D_{i,\mathrm{m1}}$ and $D_{i,\mathrm{m2}}$) is expressed by

$$\varrho_1 D_{i,\mathrm{m1}} \frac{X_i - X_i^*}{M_1 \Delta x_1} = \varrho_2 D_{i,\mathrm{m2}} \frac{Y_i^* - Y_i}{M_2 \Delta x_2} \tag{18}$$

The equilibrium data from Springer et al. [10] at 30 °C and from Hinatsu et al. [13] at 80 °C were used to complete this interfacial mass transfer model by relating the molar fraction of water of each phase at the interface ($Y_i^*$ and $X_i^*$).

### 2.4. Electrochemical model

The electrochemical kinetic was determined by using the agglomerate model [14–18]. The agglomerate model states that the catalyst layer is a porous medium composed by platinum and carbon particles mixed together with polymer electrolyte. This mixture is defined as spherical agglomerates, which have void spaces between them. In this work, the polymer electrolyte is assumed as Nafion, the water is assumed to be produced in gas phase and condensation could take place in this medium. The anode reaction is assumed to be dominated by the cathode reaction kinetic, and so, the reaction rate is finally expressed as

$$r_{\mathrm{H^+}} = \frac{3 D_{\mathrm{agg}} C_{\mathrm{O_2 s}} (1-\epsilon)}{R_{\mathrm{agg}}^2} (\theta R_{\mathrm{agg}} \coth \theta R_{\mathrm{agg}} - 1) \tag{19}$$

with the Thiele Modulus ($\theta R_{\mathrm{agg}}$) defined as

$$\theta R_{\mathrm{agg}} = \sqrt{\frac{m_{\mathrm{pt}} A_{\mathrm{superf}} i_{\mathrm{oref}}}{F D_{\mathrm{agg}} C_{\mathrm{O_2 ref}}}} R_{\mathrm{agg}} \exp\left(-\frac{\alpha_{\mathrm{c}} F \eta}{2RT}\right) \tag{20}$$

The Henry constant for the dissolution of oxygen in water is used to calculate the concentration at the surface of the agglomerate [19]:

$$C_{\mathrm{O_2 s}} = x_{\mathrm{O_2}} \frac{P}{101325} \exp\left(\frac{666}{T} - 14.1\right) \tag{21}$$

The reference exchange current density for the oxygen reduction in Nafion ($i_{\mathrm{oref}}$) is calculated by the correlation presented by Wang et al. [14] made from experimental data [20]:

$$\log(i_{\mathrm{oref}}) = 7.507 - \frac{4001}{T} \tag{22}$$

The diffusivity of oxygen in Nafion is calculated from the correlation presented by Marr and Li [16], which is made from experimental data [20]. Then, the oxygen diffusivity in the agglomerate $D_{\mathrm{agg}}$ is expressed as

$$D_{\mathrm{agg}} = \left(-1.07 \times 10^{-5} + 9.02 \times 10^{-6} \exp\left(\frac{T - 273}{106.7}\right)\right) \epsilon^{1.5} \tag{23}$$

To account for the voltage losses which are induced by the Nafion resistance to the transport of protons to the active sites, a one dimensional expression of Ohm's law is defined to estimate the increase of the cathode overpotential in the cathode catalyst layer:

$$k_{\mathrm{H^+}} ((1-\epsilon)\epsilon_{\mathrm{agg}})^{1.5} \frac{\delta \eta}{\delta x} = N_{\mathrm{H^+}} F \tag{24}$$

where $k_{\mathrm{H^+}}[\Omega^{-1}\mathrm{m}^{-1}]$ is the proton conductivity in Nafion expressed as [10]

$$k_{\mathrm{H^+}} = (0.5139\lambda - 0.3260) \exp\left(1268 \left(\frac{1}{303} - \frac{1}{T}\right)\right) \tag{25}$$

To calculate the fuel cell potential, the cathode overpotential and the polymer membrane voltage loss are subtracted from the equilibrium potential. The voltage loss produced by the bipolar plates and the contact resistance between the gas channel ribs and gas diffusion layers was neglected:

$$E = 1.23 - 9 \times 10^{-4}(T - 298) + \frac{2.3RT}{4F} \log(P_{\mathrm{H_2}}^2 P_{\mathrm{O_2}}) - \eta - \frac{i}{k_{\mathrm{H^+}}} \tag{26}$$

### 2.5. Source terms

The pressure drop in gas channels was estimated using the Darcy friction factor, and so, the implementation of the SIMPLE algorithm [21] was avoided. Therefore, only diffusion is assumed to be the primary mechanism in gas diffusion layers and catalyst layers while convection is neglected. According to this assumption, the source term of momentum $S_V$ in the porous mediums is not considered in Eq. (1), and so, the Navier–Stokes equations are only used in the gas channels without source terms. The source term of mass $S_{\mathrm{m}}$ in Eq. (4) was also neglected following the demonstration made by Wang and Wang [22].

Joule heating in the polymer membrane, heat produced in cathode reaction and heat produced in condensation–evaporation entropy change are taken into account as source terms of energy $S_T$ in Eq. (2). The Joule heating $S_{T1}$ in the membrane is calculated by using the proton conductivity in Nafion and the proton flow as follows:

$$S_{T1} = \frac{(N_{\mathrm{H^+}} F)^2}{k_{\mathrm{H^+}}} \tag{27}$$

The heat produced in the cathode reaction is determined using the reaction heat of oxygen reduction $\Delta Hr_{O_2}$ and the reaction rate:

$$S_{T2} = \Delta Hr_{O_2} r_{O_2} \quad (28)$$

And the condensation–evaporation entropy change in the cathode porous mediums is estimated using the latent heat of vaporization of water at local temperature $H_{LG}$ and the volumetric condensation rate:

$$S_{T3} = H_{LG} \dot{n}_{GLH_2O} \quad (29)$$

The electrochemical reaction in the catalyst layers is considered as the source term of species i $S_i$ in Eq. (3):

$$S_i = M_i r_i \quad (30)$$

The reaction rate of every species is obtained from the one expressed in Eq. (19) using the stoichiometrical relations derived from the well-known mechanism of reaction in PEM fuel cells.

Finally, the condensation and evaporation process in the cathode porous medium is considered as additional source term for the water gas balance:

$$S_{H_2O} = \dot{n}_{GLH_2O} \quad (31)$$

It is important to mention that every source term is activated only in its defined domain.

## 3. Results and discussion

In PEM fuel cells, there are many parameters that may affect their performance either slightly or heavily. These parameters may be separated into three sections: the geometrical, the electrochemical and the operational. The geometrical and electrochemical parameters arbitrarily used in this work are listed in Table 1.

The principal aim is the study of the behavior of the polymer membrane water content, the saturation in the cathode porous medium and the cathode reaction rate, in order to establish the influence of these factors on the performance of fuel cells under different operational conditions. The results are mostly presented as transversal averages along the gas channels, given that the three-dimensional displays are not practical to make comparisons.

Table 1
Geometrical and electrochemical parameters

| Description | Value |
|---|---|
| Channel height (m) | 0.0004 |
| Channel width (m) | 0.001 |
| Channel length (m) | 0.10 |
| Channel rib (m) | 0.0004 |
| Gas diffusion layer thickness (m) | 0.0001 |
| Gas diffusion layer porosity | 0.5 |
| Catalyst layer thickness (m) | 0.000001 |
| Catalyst layer porosity | 0.4 |
| Polymer membrane thickness (m) | 0.00023 |
| Pt loading ($mg_{Pt}cm^{-2}$) | 1 |
| Pt surface area ($cm^2_{Pt}g_{Pt}{}^{-1}$) | 250000 |
| Agglomerate porosity | 0.2 |
| Agglomerate radii (cm) | 0.00001 |
| Reaction heat ($J\,mol^{-1}$) | 460000 |

### 3.1. Water content field at different current densities

The magnitude of the current density may affect the water content field of the polymer membrane. Therefore, the local current density and the local water content along the channel were computed at different total average current densities and fully humidified inlet flows (Fig. 2(A) and (B), respectively). In Fig. 2(A), it can be seen that the local current density diminishes along the channel, because of the depletion of oxygen by the cathode reaction. The local water content increases along the channel, given the increase of water activity, as a result of the production of water by the electrochemical reaction in the cathode (Fig. 2(B)). The reaction at the anode also contributes to the increase of the water activity at this side, due to the fully humidified condition of the anode inlet flow and the consumption of hydrogen along the channel. Consequently, the water molar fraction increases along the channel at the anode side. The increase of water content becomes slower towards the end of the channel, as a product of the consumption of oxygen along the channel and so the reduction of the cathode reaction rate. Due to the fully humidified condition of the inlet flows, the electro-osmotic drag is insufficient to dry the anode side of the polymer membrane, even for high current densities. Under these conditions the cell voltage is only affected by the proton flux and not by the water content of the polymer membrane.

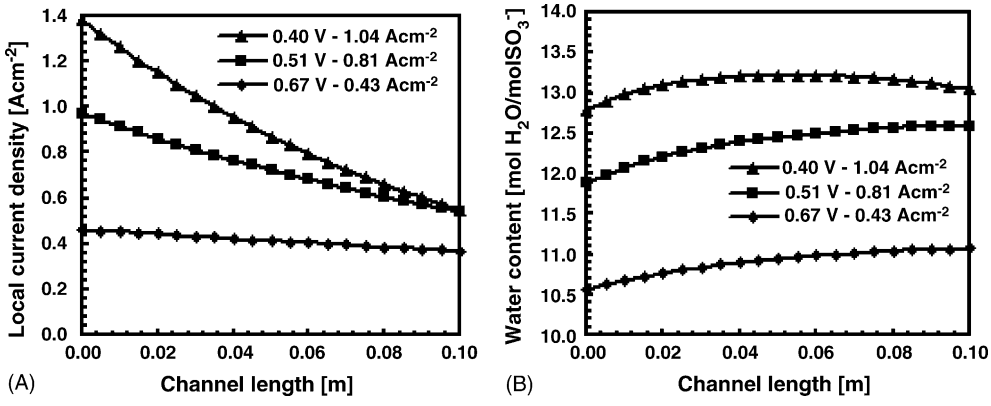


Fig. 2. (A) Current density and (B) membrane water content along the channel for different average current densities.

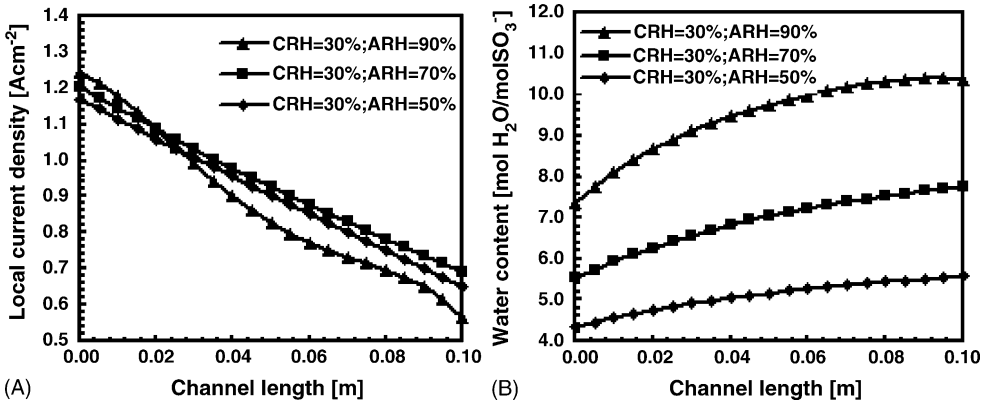


Fig. 3. (A) Current density and (B) membrane water content along the channel for different relative humidities of anode inlet flow.

### 3.2. Effect of the cathode and anode inlet flow relative humidity

As mentioned above, once the inlet flows are fully humidified, the water content of the polymer membrane is favored, and consequently, the performance of the fuel cell is not affected by the hydrating conditions of the electrolyte. However, the relative humidity of the cathode inlet flow may have a considerably influence on the performance of the fuel cell. In case the inlet flows are not well humidified, voltage losses from the electrolyte may increase and have a high negative influence on the cathode reaction rate, as a result of the decrease of proton conductivity of the polymer electrolyte, which depends linearly on the water content. If the water content decreases, then the cathode overpotential increases, due to the increment of proton resistance, and so the cathode reaction rate. The voltage loss induced by the polymer membrane is also increased, as product of the dehydrating conditions.

The relative humidity of cathode and anode inlet flows were varied at high current density operation, in order to study the performance of the fuel cell under dehydrating conditions. The relative humidity of the cathode inlet flow is maintained at 30% and the anode inlet flow presents relative humidity of 50, 70 and 90%. Fig. 3(A) shows that the local current density diminishes along the channel, as a result of the decrease of oxygen concentration. The effect of the electrolyte on the current density is slightly seen for the anode relative humidity of 90%, given that the current density is higher at the gas channel inlet. However, the oxygen is faster consumed, and so, the local current density is less in comparison to the 50 and 70% relative humidity. The local water content increases along the channel (Fig. 3(B)), consequently the electrolyte limitations at the cathode catalyst layer decrease as well. In this case, the anode relative humidity enhances the hydration of the polymer membrane. Under these conditions it can be seen that the effect of the polymer electrolyte on the current density is small in comparison to the effect of the oxygen mass transfer limitations and depletion.

To study the potential effect of Nafion in the cathode electrode on the reaction, the thickness of the cathode catalyst layer was made thicker (by a factor of 10), maintaining the superficial platinum load constant, in order to increase the proton transport resistance in comparison to the reaction rate. The results are showed in Fig. 4(A) and (B) at the same humidity conditions used for Fig. 3. Fig. 4(A) shows the current density along the channel for dehydrating conditions. It can be seen that for low water content of polymer, the resistance of the Nafion to the proton transport becomes high and affects the performance of the fuel cell so as the oxygen mass transfer limitations do. In this case, the current density slightly increases along the channel, given that the water content of the electrolyte becomes higher as result of the production of water by the cathode reaction (Fig. 4(B)). Then, the oxygen mass transfer limitation and the decrease

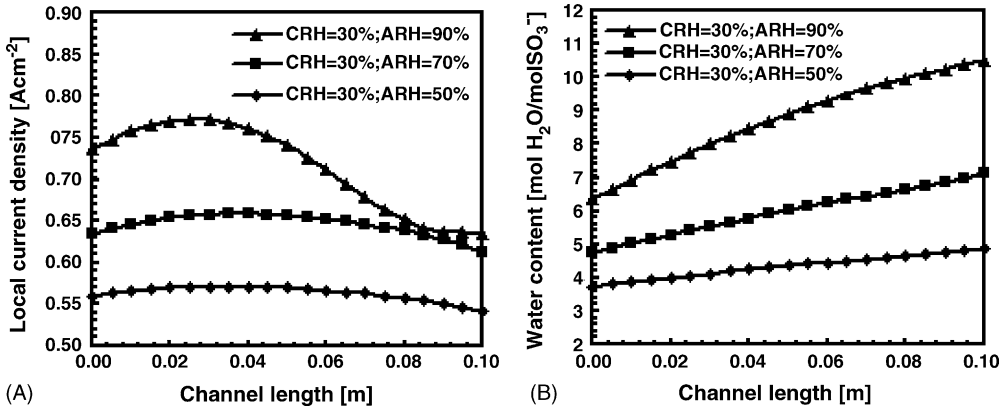


Fig. 4. (A) Current density and (B) membrane water content along the channel for different relative humidities of anode inlet flow.

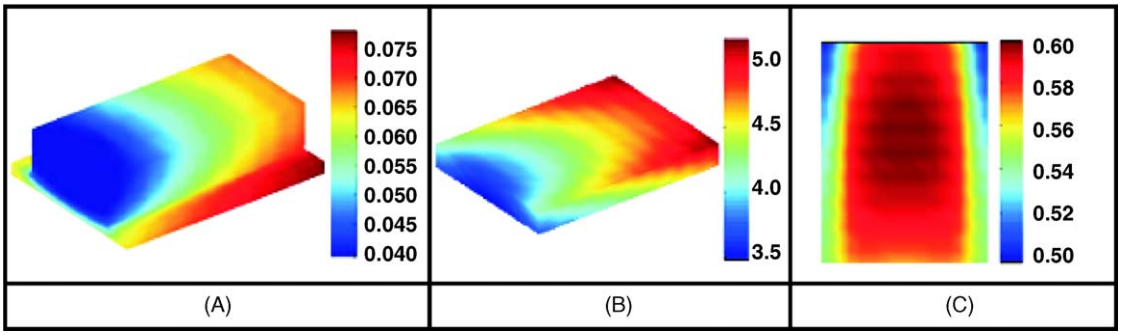


Fig. 5. Maps of (A) vapor mass fraction, (B) polymer membrane water content field and (C) current density.

of the oxygen concentration reduce the reaction rate, despite the hydration of the polymer membrane and the electrolyte in the cathode catalyst layer. Fig. 5 shows the cathode water vapor mass fraction, the water content field for relative humidity of cathode and anode inlet flows at 30 and 50% (respectively) and the current density. As it can be seen, the maximal current density area has moved towards the end of the channel, as a result of the better hydration of the electrolyte by the electrochemical reaction. However, this area is closed, because of the decrease of the oxygen concentration along the channel.

### 3.3. Water saturation of the cathode porous medium

The cathode saturation represents one of the most important problems to consider, given that the liquid water may block the path of reactants to the active sites. Therefore, the inlet relative humidity improves the electrolyte performance of the fuel cell, but may decrease the flux for the diffusion to active sites. The saturation should be quantitatively estimated to avoid the flooding in the cathode side by an incorrect water management.

The saturation in the cathode porous medium may be affected by several factors: current density, temperature of operation, hydrophobicity and permeability of porous medium and relative humidity of cathode and anode inlet flows. The condensation and evaporation process depends highly on the interfacial area between the gas and the liquid. To predict an accurate value for the volumetric interfacial area is a difficult task, especially for the complexity of the three-phase system. As mentioned above, the volumetric interfacial area is arbitrarily considered as a constant parameter during the condensation and evaporation process.

The saturation of the porous medium becomes a problem when the system is unable to dispose the liquid water product from the excess of water vapor at the same speed it is produced by the cathode reaction. Therefore, the liquid water accumulates and the available area for the diffusion is reduced. Then, high voltage losses occur, because of the high mass transfer control from the high mechanical resistance for diffusion. However, once the water accumulates, some continuous liquid water paths will be formed and there will be a capillary flow straight to the gas channel, so that the liquid water can be disposed. This phenomenon may keep the system from flooding, although the mass transfer control may remain.

In this work, the influence of the volumetric interfacial area on the performance of the fuel cell was computed by assuming different values of this parameter. Fig. 6(A) and (B) show the local saturation and water content along the channel for volumetric interfacial areas of 1000, 10,000 and 50,000 $m^2\ m^{-3}$ at high current densities and fully humidified inlet flows, respectively. It can be observed from Fig. 6(A) that the amount of liquid water is slightly governed by the effect of the interfacial area, for the values chosen in this work. According to these results, the system is able to get rid of the water and the maximal saturation is approximately below the value of 0.2 at the cathode catalyst layer. Consequently, the capillary flow controls the saturation process against the condensation and evaporation process. In this case

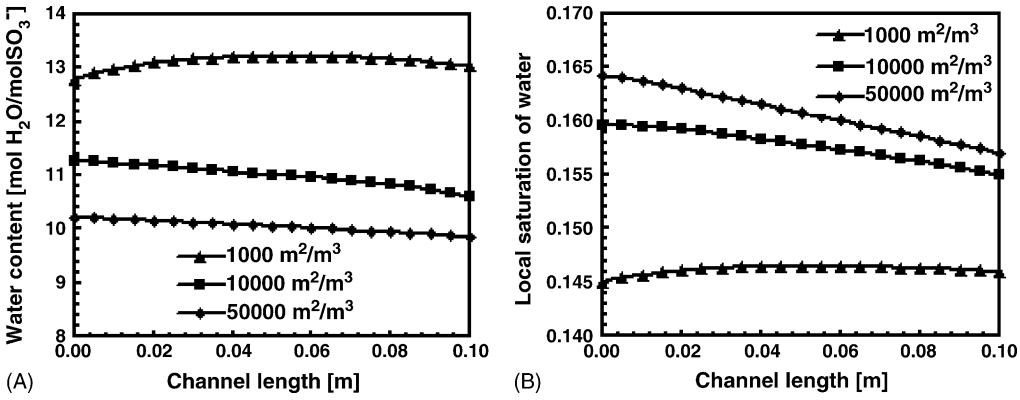


Fig. 6. (A) Membrane water content and (B) saturation along the channel at different volumetric gas–liquid interfacial areas.

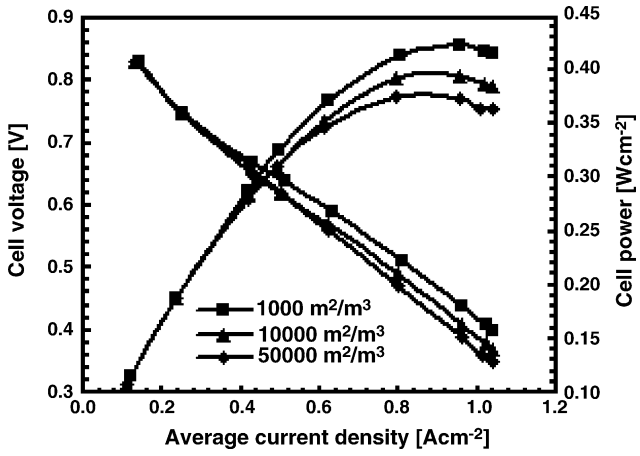


Fig. 7. Cell voltage and power vs. average current density at different volumetric gas–liquid interfacial areas.

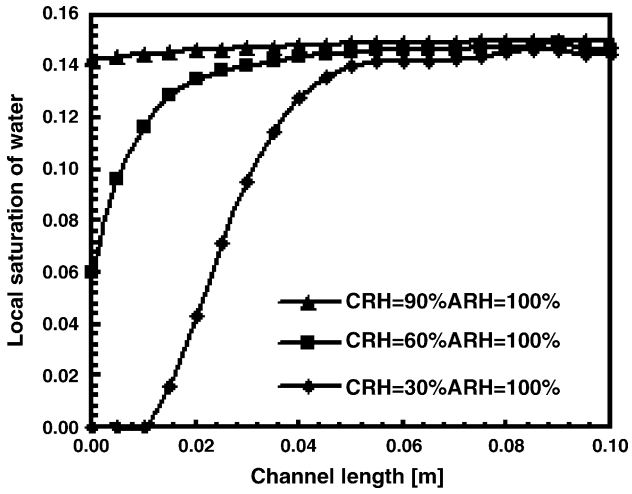


Fig. 8. Saturation along the channel at different cathode inlet flow relative humidity.

the dominating effect is neither the volumetric interfacial area nor the current density of the fuel cell, but the permeability and hydrophobicity of the porous medium. It can also be seen from Fig. 6(A) how the average saturation changes along the channel. This factor increases as a result of the increase of water activity along the channel. The saturation tends to reach a maximum, given the decrease of reaction rate towards the channel. The water content could be affected by the volumetric interfacial area of the gas and liquid interface, as it can be seen in Fig. 6(B). The local water content decreases with increasing volumetric interfacial area. Therefore, the higher condensation of water vapor reduces the mass of water that may be transferred to the polymer electrolyte. Consequently, the voltage loss in the polymer membrane may be affected by the higher volumetric interfacial area.

Fig. 7 shows the cell voltage and power vs. average current density for volumetric interfacial areas of 1000, 10,000 and 50,000 $m^2\,m^{-3}$. As it can be seen for high current densities, fuel cell voltage decreases while volumetric interfacial area increases. Therefore, under these conditions the current density is not seriously affected by saturation of liquid water in the cathode electrode, given that the difference of the saturation magnitudes is small for all cases. The significance of this behavior may be the low mass transfer control that liquid water induces in the cathode porous medium in comparison to the resistance that the porous medium exerts on the diffusive flux. The performance of the fuel cell is mainly decreased by the influence of the volumetric interfacial area on the water uptake of the polymer membrane, and so on voltage of the fuel cell. Nevertheless, the water uptake from liquid water is neglected and this factor might be important to obtain more accurate results for the water uptake of the polymer membrane.

To study the influence of the cathode inlet relative humidity on the liquid saturation of the cathode porous medium, different curves were computed at 30, 60 and 90% cathode relative humidity maintaining the anode relative humidity at 100% and the volumetric interfacial area at 1000 $m^2\,m^{-3}$ (Fig. 8). In this case the relative humidity has a strong influence on the condensation and evaporation process, due to the unsaturation of the inlet flow. Then, there will be a tendency to evaporation at the gas channel and cathode gas diffusion layer, and so the dispose of water is made by change of phase and not by the drag of liquid droplet in the gas channel. For higher inlet humidity the capillary flow dominates against the evaporation, and so the disposal is made by the mechanical energy of the flow in the gas channel.

The relation of local temperature and liquid saturation of the cathode porous medium is also to be accounted for. Fig. 9 shows the distributions of temperature and liquid saturation in the through-plane direction along the channel right in the middle of the fuel cell for fully humidified inlet flows and high current density operation (1.04 $A\,cm^{-2}$). For fully humidified inlet flows, reaction rate is higher at the entrance and diminishes along the channel by depletion of reactants. Likewise temperature is higher at the entrance and becomes lower along the channel (Fig. 9(A)). In through-plane direction, temperature diminishes towards the gas channel due to convection in the interface between gas channel and gas diffusion layer. According to the distribution of temperature, the convection in gas channels maintains the cell almost at uniform temperature. Under the conditions listed in Table 1, the heat of reaction and Joule heating are not high enough to increase considerably the temperature against convection in gas channels. In the case of the local saturation, the distribution (Fig. 9(B)) depends not only on temperature distribution, but also on water vapor mass fraction distribution and capillary flow. Fig. 9(B) shows that the local liquid saturation slightly increases along the channel and slightly decreases in through-plane direction towards the gas channel. Thus, as mentioned above capillary flow plays the most important role on the liquid distribution. Even though water activity may change almost 100% along the channel (as it can be seen in Fig. 5(A)), local saturation is almost homogeneous in cathode porous medium due to the capillary flow. The lower liquid saturation after the entrance of fuel cell shows that temperature and water activity distributions have an influence on the distribution of saturation; however these effects are small in comparison to the capillary flow.

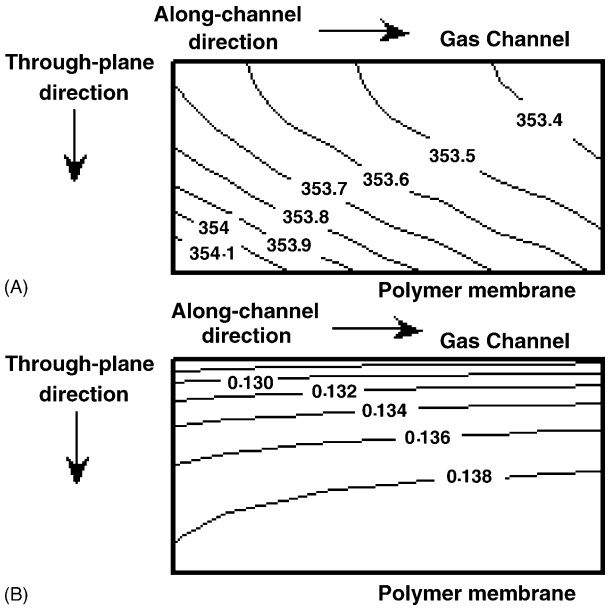


Fig. 9. Through-plane and along-channel distributions of (A) temperature and (B) liquid saturation.

### 3.4. Effect of the operational temperature

To observe the influence of the operational temperature on the performance of the fuel cell, the local water content and the current density along the channel were computed for 70, 80 and 90 °C (Fig. 10(A) and (B), respectively). From Fig. 10(A), it can be seen that the local current density decreases while the temperature increases. This effect is especially seen for the results of 90 °C. Therefore, the performance of the fuel cell diminishes at higher temperatures for fully humidified inlet flows, as a result of the influence of the temperature on the hydration of the polymer electrolyte, as it can be seen in Fig. 10(B). For the temperature of 90 °C, the water content of the polymer membrane dramatically diminishes for fully humidified inlet flows, and so the electrolyte overpotential increases. Hence, the temperature may have a positive effect on the reduction of the oxygen, but the higher proton resistance produced by the electrolyte dehydration at high temperatures has a dominant influence on the cathode reduction reaction.

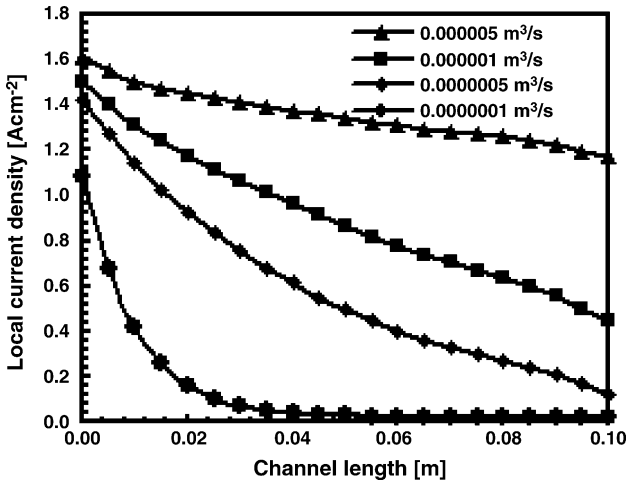


Fig. 11. Current density along the channel at different cathode inlet volumetric flows.

### 3.5. Effect of cathode inlet volumetric flow

At high current densities, the demand of oxygen is high, and so the inlet flow should be able to supply the needed amount of oxygen. In the case the oxygen is gradually depleted, the performance of the fuel cell diminishes, due to the high cathode overpotential induced by the lack of oxygen. Fig. 11 shows the local current densities along the channel at different cathode inlet volumetric flows. The results show the high influence of the oxygen concentration on the cathode reaction rate. Even for the highest inlet volumetric flow, the drop of the current density along the channel is noticeable along the channel. Nevertheless, the channel length was arbitrarily chosen and the aim of this calculation is to show how the depletion of oxygen may affect the performance of the fuel cell at different current densities.

### 3.6. Comparisons to the experimental data

The validation of the data is an obliged step of every either experimental or numerical work. Considering that each author has made emphasis on different aspects of the PEM fuel cells, the comparison between numerical models becomes useless. Given that the properties fields are not experimentally measured in

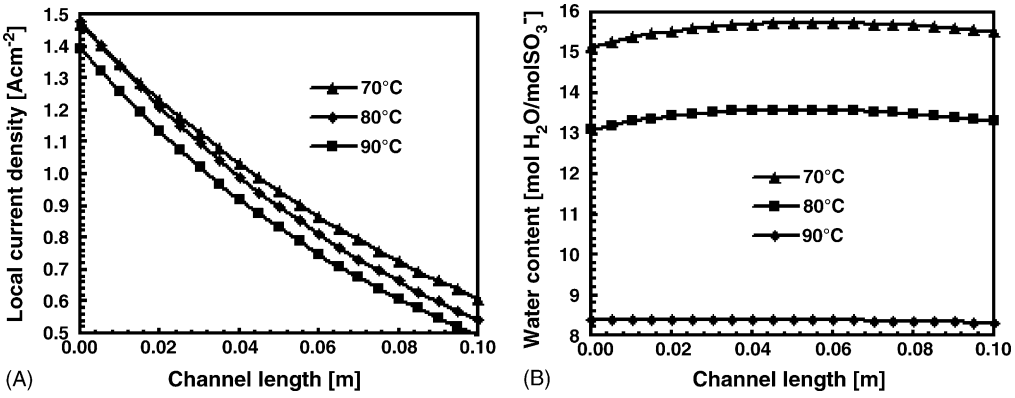


Fig. 10. (A) Membrane water content and (B) saturation along the channel at different operation temperature.

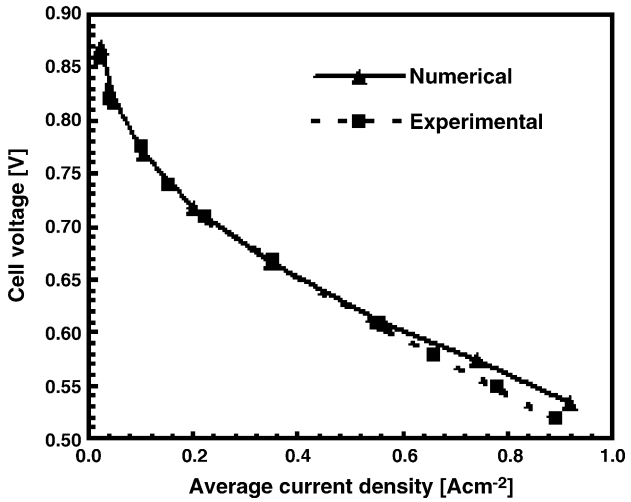


Fig. 12. Experimental [23] and numerical polarization curves.

the literature, but numerically calculated, only the experimental polarizations (cell voltage versus average current density) could be taken as reliable sources to make comparisons. The shape of a polarization curve is highly influenced at low and moderates current densities by the electrochemical reaction rate, but at high current densities, the voltage loss in the polymer membrane also plays an important role. These factors are highly sensible to the electrochemical parameters (listed in Table 1) and the proton conductivity and thickness of the polymer membrane, and so, it is necessary to point out that the success of the validation depends on the use of the correct electrochemical input data and the correct polymer membrane characteristics. Additionally, the geometrical parameters should be as close as possible to the parameters of the experimental setup used as reference. In this work, the numerical input data were adjusted as close as possible to the conditions of the experimental data from [23], in order to validate the numerical solution. The comparison between the experimental polarization curve at 80 °C and 200 kPa and the numerical one (Fig. 12) shows that the numerical solution is suitable for studying the water and heat behavior in PEM fuel cells.

## 4. Conclusions

A three-dimensional model for a PEM fuel cell was programmed in Fortran90 to achieve a numerical solution of the water and heat behavior, in order to analyze the factors that may be either positive or negative for the performance of this technology. Under the conditions and geometry chosen in this work, the system showed to be highly dependant on the hydration of the polymer membrane, which was affected by the relative humidity of the inlet flows. The saturation of the cathode porous medium was dominated by the capillary flow, and so, the permeability was high enough to dispose the water in the system. The volumetric interfacial area of the water affected the performance of the fuel cell by reducing the amount of water to be transferred to the polymer membrane. The operational temperature may have a negative effect on the hydrating properties of the polymer electrolyte, and so on the performance of the fuel cell, especially for values above 90 °C. The saturation of the cathode porous medium was not dramatically affected by the operation conditions and its magnitude did not overcome the value of 0.2. Then, the capillary flow was high enough to dispose the produced water and to prevent the system from flooding. The chosen experimental polarization curve was in good agreement with the calculated one. This numerical solution constitutes a useful tool for studying the behavior of PEM fuel cell under several conditions. The characteristics of the materials that compose "MEA" can also be varied to extend the possibilities of this solution. For further research, this numerical solution can be adapted to more complex geometries (serpentine and interdigitated flow fields). The estimation of the efficiency for different configurations is also an aspect to consider for future aims.

## References

[1] C. Heller, Modellbildung, Simulation und Messung thermofluiddynamischer Vorgänge zur Optimierung des Flowfields von PEM-Brennstoffzellen, in: D. Brüggemann (Ed.), Thermodynamik: Energie, Umwelt, Technik, vol. 7, Logos-Verlag, Berlin, 2004.
[2] U. Pasaogullari, C.-Y. Wang, Two-phase modeling and flooding prediction of polymer electrolyte fuel cells, J. Electrochem. Soc. 152 (2) (2005) A380–A390.
[3] C.-Y. Wang, Fundamental models for fuel cell engineering, Chem. Rev. 104 (10) (2004) 4727–4766.
[4] Z.H. Wang, C.Y. Wang, K.S. Chen, Two-phase flow and transport in the air cathode of proton exchange membrane fuel cells, J. Power Sources 94 (2001) 40–50.
[5] D. Natarajan, T. Van Nguyen, A two-dimensional, two-phase, multicomponent, transient model for the cathode of a proton exchange membrane fuel cell using conventional gas distributors, J. Electrochem. Soc. 148 (12) (2001) A1324–A1335.
[6] T. Berning, N. Djilali, A 3D multiphase, multicomponent model of the cathode and anode of a PEM fuel cell, J. Electrochem. Soc. 150 (12) (2003) A1589–A1598.
[7] J.H. Nam, M. Kaviany, Effective diffusivity and water-saturation distribution in single- and two-layer PEMFC diffusion medium, Int. J. Heat Mass Transfer 46 (2003) 4595–4611.
[8] M.M. Tomadakis, S.V. Sotirchos, Ordinary and transition regime diffusion in random fiber structures, AIChE J. 39 (1993) 397–412.
[9] R.B. Bird, W.E. Stewart, E.N. Lightfoot, Transport Phenomena, Wiley, New York, 1960.
[10] T.E. Springer, T.A. Zawodzinski, S. Gottesfeld, Polymer electrolyte fuel cell model, J. Electrochem. Soc. 138 (8) (1991) 2334–2342.
[11] W. Neubrand, Modellierung und Simulation von Electromembranverfahren, Dissertation, Universität Stuttgart, Germany, 1999.
[12] T.A. Zawodzinski, C. Derouin, S. Radzinski, R. Sherman, V.T. Smith, T. Springer, S. Gottesfeld, Water uptake by and transport through Nafion 117 membranes, J. Electrochem. Soc. 140 (4) (1993) 1041–1047.
[13] J.T. Hinatsu, M. Mizuhata, H. Takenata, Water uptake of perfluorosulfonic acid membranes from liquid water and water vapour, J. Electrochem. Sources 141 (6) (1994) 1493–1498.
[14] Q. Wang, D. Song, T. Navessin, S. Holdcroft, Z. Liu, A mathematical model and optimization of the cathode catalyst layer structure in PEM fuel cells, Electrochem. Acta 50 (2004) 725–730.
[15] F. Jaouen, G. Lindbergh, G. Sundholm, Investigation of mass-transport limitations in the solid polymer fuel cell cathode, J. Electrochem. Soc. 149 (4) (2002) A437–A447.
[16] C. Marr, X. Li, Composition and performance modeling of a catalyst layer in a proton exchange membrane fuel cell, J. Power Sources 77 (1999) 17–27.

[17] M.L. Perry, J. Newman, E.J. Cairns, Mass transport in gas-diffusion electrodes: a diagnostic tool for fuel-cell cathodes, J. Electrochem. Soc. 145 (1) (1998) 5–15.
[18] K. Broka, P. Ekdunge, Modeling the PEM fuel cell cathode, J. Appl. Electrochem. 27 (1997) 281–289.
[19] D.M. Bernardi, M.W. Verbrugge, Mathematical model of the solid polymer electrolyte fuel cell, J. Electrochem. Soc. 139 (9) (1992) 2477–2491.
[20] A. Parthasarathy, S. Srinivasan, J. Appleby, Temperature dependence of the electrode kinetics of oxygen reduction at the Platinum/Nafion interface—a microelectrode investigation, J. Electrochem. Soc. 139 (9) (1992) A437–A447.
[21] S. Patankar, Numerical Heat Transfer and Fluid Flow, Hemisphere Publishing Corporation, New York, 1980.
[22] Y. Wang, C.-Y. Wang, Modeling polymer electrolyte fuel cells with large density and velocity changes, J. Electrochem. Soc. 152 (2) (2005) A445–A453.
[23] J. Ihonen, F. Jaouen, G. Lindbergh, G. Sundholm, A novel polymer electrolyte fuel cell for laboratory investigations and in situ contact resistance measurements, Electrochem. Acta 46 (2001) 2899–2911.